# 22

# FEM Applied to Hydrodynamic Bearing Design

Fabrizio Stefani
*University of Genoa*
*Department of Mechanics and Machine Design*
*Italy*

## 1. Introduction

Nowadays hydrodynamic lubrication analysis involves sophisticated models that use a large number of variables. For instance the evaluation of temperatures, which directly determine the viscosity of the lubricant fluid and hence its load carrying capacity, has become a standard procedure and the related analysis type is referred to as *ThermoHydroDynamic* (THD) analysis. *ThermoElastoHydroDynamic* (TEHD) models introduce a further enhancement in lubrication analysis by including the simulation of bearing deformations due to mechanical loads and/or thermal effects.
TEHD lubrication is an interdisciplinary field including structural, thermal, thermo-elastic and hydrodynamic simulations. Hence it requires a multi-physic approach that should be based on a well-rounded discretization technique capable of simplifying the simultaneous management of different interconnected models, which must exchange data between themselves. This task is well-accomplished by the Finite-Element Method (FEM), an overall discretization technique particularly suited for problems with complicated integration domains and non-smooth solutions.
A TEHD model of a kinematic pair simulates the thermal and mechanic interaction among the lubricant film and the lubricated solid members. As far as the fluid film sub-model is concerned, it must rely on the mass and energy conservation principles. The separation of the fluid (cavitation) in the divergent film region and the presence of feed grooves on bearing surfaces encumber the formulation of the conservation principles especially in the finite-element perspective and require special modelling techniques.
The present chapter is aimed to provide the theoretical foundation of FEM mass- and energy-conserving models as well as to report their application to the THD and/or TEHD analysis of different bearing types. Author's original contributions to the simulation methods are explained. They include the FEM groove-mixing theory, the SUPG stabilization of the conservation equations and the "quasi-3D" approach to the thermal problem. The theoretical construct is useful to enable the analysts to manage the models and to understand the responses. The application examples are relevant to both journal and axial bearings with fixed and tilting pads, in order to demonstrate the high flexibility of the method. With few modifications the presented method can be applied to the design of several types of bearings in both steady and dynamic loading conditions. The scope of the paper is anyway limited to the analysis of steadily-loaded bearings working in laminar lubrication regime.

## 2. State-of-the-art

Modern lubrication analysis methods enable us to assess bearing performances with high accuracy. By taking advantage of detailed THD simulations the maximum deviation between experimental findings and numerical predictions for white metal temperatures may be less than 3-4°C (Banwait & Chandrawat, 1998).
TEHD analysis is compulsory in order to achieve sufficiently reliable results for highly loaded journal bearings (Bouyer & Fillon, 2004), tilting pad journal bearings (Chang et al., 2002), thrust bearings (Brugier & Pasal, 1989) and dynamically loaded supports (i.e. big end bearings of connecting rods for automotive engines) (Piffeteau et al., 2000). TEHD analysis may also be convenient in the case of journal bearings with stiff housing (i.e. for turbomachineries) in order to avoid assumptions about the effective clearance in working conditions.
FEM is more and more often used in lubrication analysis (Booker & Huebner, 1972; Bonneau & Hajjam, 2001). A FEM version of the classic groove-mixing theory (Robinson & Cameron, 1975) is explained in the following. It has been developed by formulating the energy balance for the supply grooves at the element level, in order to deal with all of the lubrication problem details in finite-element terms.
Suitable stabilization techniques are compulsory in lubrication analysis to solve by means of FEM the energy and the cavitation equations, whereas they rule parabolic and hyperbolic differential problems, respectively. The Streamline Upwind Petrov-Galerkin (SUPG) technique (Kelly et al., 1980; Tezduyar & Sunil, 2003), applied by the author to both problems, is fully explained in the following. Although more straightforward upwinding techniques have been initially proposed by other authors (Kumar & Booker, 1991), SUPG is more general, as it does not depend on the element type.
As convection is the main mechanism of heat exchange in the lubricant film, oil temperatures and flows are directly related. Hence a consistent treatment of the thermal problem demands an equally reliable model of film hydrodynamics.
In this perspective the FEM mass-conserving algorithms developed in the last decade by researchers (Kumar & Booker, 1991; Bonneau & Hajjam, 2001) are an essential tool to provide the accurate estimate of the lubricant flow needed by THD and TEHD analysis methods. A mass- and energy-conserving FEM model has been presented by Kumar & Booker (1994). The resulting algorithm is fast as it turns the three-dimensional (3D) thermal problem in a two-dimensional (2D) one by solving the energy equation averaged across the film thickness and by assuming adiabatic walls. Afterwards such a method has been enhanced in a previous work (Stefani & Rebora, 2009), where it is incorporated in a complete 3D TEHD simulation and it is completed with boundary conditions consistent with the continuity of mass and energy throughout the integration domain.
To this purpose the temperature variation across the film thickness is calculated by fitting the temperature profile with a fourth-order polynomial (quasi-3D approach) and the above-mentioned groove-mixing theory is employed. In such an arrangement the algorithm has shown good agreement with experimental results. The computational cost is still reasonable and the algorithm is very flexible and well-suited to different bearing types and geometries. Consequently the model can serve as the basis for codes dedicated to bearing design and verification for industrial purposes.

## 3. Basic equations

### 3.1 Thin film mechanics equations

In kinematic pairs working in hydrodynamic and elastohydrodynamic lubrication regime, the lubricant action is exerted through a thin film between two members (with facing surfaces 0 and 1) in motion at velocity $\mathbf{V_0}$ and $\mathbf{V_1}$, respectively (Fig. 1).

The following usual "Reynolds hypotheses" are assumed. The lubricant is Newtonian and it flows in laminar regime in the narrow clearance between the two members, with no-slip conditions at the walls. The film curvature yields negligible effects.

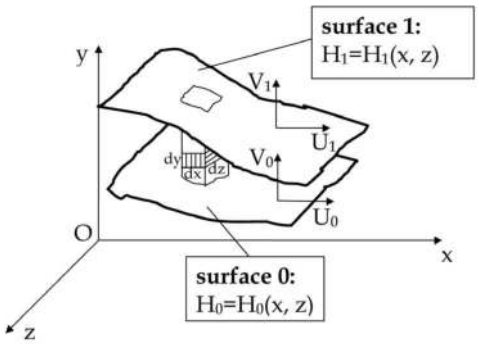


Fig. 1. Reference system O(x, y, z) and flow between the two surfaces 0 and 1 moving with velocity $\mathbf{V_0}$={$U_0$, $V_0$, 0} and $\mathbf{V_1}$={$U_1$, $V_1$, 0}

The velocity distributions of the fluid into the film thickness can be obtained from the Navier-Stokes equations, simplified by means of the above-mentioned assumptions and integrated with suitable boundary conditions (the fluid velocity at the surfaces 0 and 1 are $\mathbf{V_0}$ and $\mathbf{V_1}$, respectively). After velocity is substituted in the continuity equation, its integration in a columnar element of fluid (Fig. 1) with height H = $H_1$ – $H_0$ and rectangular basis dx · dz provides the thin film mechanics equation, also referred to as Reynolds generalized equation, (Dowson, 1967). At time t, for a full film of compressible fluid developed in a rectangular domain, where a cartesian coordinate system O(x, y, z) is fixed, it states

$$\frac{\partial}{\partial x}\left(\rho g\frac{\partial p}{\partial x}\right)+\frac{\partial}{\partial z}\left(\rho g\frac{\partial p}{\partial z}\right)=\frac{\partial}{\partial x}\left\{\rho\left[U_1H_1-U_0H_0-f\left(U_1-U_0\right)\right]\right\}+\frac{\partial}{\partial t}\left(\rho H\right) \tag{1}$$

where the hydrodynamic pressure p as well as the fluid density ρ are independent of the y coordinate and

$$\left.\begin{aligned} f &= i_1 / i_0 \\ g &= i_2 - {i_1}^2 / i_0 \end{aligned}\right\} \tag{2}$$

with

$$i_s=\int_{H_0}^{H_1}\frac{y^s}{\mu}\,dy \tag{3}$$

The lubricant viscosity $\mu$ (eq. (3)) is variable along the film thickness (with the y coordinate) as well as in the bearing surface (with the x and z coordinates).
Although equation (1) is time dependent, it is not referred to as the equation of the thin film dynamics, as inertia and volume forces are negligible in a thin film. Hence the reference frame O(x, y, z) can be chosen regardless of whether it is inertial or not.
In order to express eq. (1) in a form useful for bearing analysis, the plane y=0 is assumed to lie on the surface 0. Therefore equations of surfaces 0 and 1 become $H_0 = 0$ and $H_1 = H$, respectively. In addition, let O(x, y, z) be fixed to surface 0, namely surface 0 is steady in this reference frame. Hence, if U is the relative velocity between surface 1 and surface 0, the kinematic terms in eq. (1) are $U_0=0$ and $U_1=U$.
These assumptions simplify the thin film mechanics equation as follows

$$\frac{\partial}{\partial x}\left(\rho g\frac{\partial p}{\partial x}\right)+\frac{\partial}{\partial z}\left(\rho g\frac{\partial p}{\partial z}\right)=\frac{\partial}{\partial x}\left[\rho U\left(H-f\right)\right]+\frac{\partial}{\partial t}\left(\rho H\right) \tag{4}$$

Equation (4) may be used for analysis of journal bearings, when their geometry and operating conditions enable Reynolds hypotheses to be fulfilled. As curvature effects are neglected the x axis is set in circumferential direction ($x = R\,\vartheta$, where R is the shaft radius).
In order to avoid the simulation of moving grooves, the surface where feed holes and/or lubricant supply grooves are machined is chosen as surface 0. Usually surface 0 and surface 1 lie on the bush and the journal respectively, as in the case of rotor journal bearings, submitted to steady loads and fed through suitable grooves in the bushing. In big end bearings of connecting rods for internal combustion engines, working under dynamic loads, the feed holes are machined in the crankshaft. Hence the sleeve wall may be chosen as surface 0 only if it houses a circumferential groove. Otherwise surface 0 is chosen on the journal, and U becomes the velocity of the bearing with respect to the journal. Nevertheless, as this chapter focus more specifically on rotor bearings, the reference surface 0 for radial bearings will be always on the sleeve in the following. Consequently, if $\omega$ is the shaft rotation speed (with respect to the bearing), $U = \omega R$.
The relative surface velocity U (or $\omega$) may either depend or not depend on the x (or $\vartheta$) coordinate as for journal bearings submitted to either dynamic or steady loads, respectively. In the former case such a dependency yields higher order infinitesimal in eq. (4) and it can be neglected in the simulation of the thin film mechanics.
The resulting form of the thin film mechanics equation for journal bearings is

$$\frac{1}{R^2}\frac{\partial}{\partial \vartheta}\left(\rho g\frac{\partial p}{\partial \vartheta}\right)+\frac{\partial}{\partial z}\left(\rho g\frac{\partial p}{\partial z}\right)=\omega\frac{\partial}{\partial \vartheta}\left[\rho\left(H-f\right)\right]+\frac{\partial}{\partial t}\left(\rho H\right) \tag{5}$$

In the annular domain, where the lubricant film develops in the case of thrust bearings, the coordinate frame used to locate a generic point Q (Fig. 3) is the cylindrical coordinate system O(r, y, $\vartheta$). An analogous integration of the Navier-Stokes and continuity equations in the reference frame O(r, y, $\vartheta$), leads to

$$\frac{1}{r}\frac{\partial}{\partial \vartheta}\left(\frac{\rho g}{r}\frac{\partial p}{\partial \vartheta}\right)+\frac{1}{r}\frac{\partial}{\partial r}\left(\rho g r\frac{\partial p}{\partial r}\right)=\omega\frac{\partial}{\partial \vartheta}\left[\rho\left(H-f\right)\right]+\frac{\partial}{\partial t}\left(\rho H\right) \tag{6}$$

By taking advantage of a conformal mapping technique (Wang et al., 2003), in agreement with the coordinate transformation $z = R\ln(r/R)$ (R is the inner pad radius, shown in Fig. 3),

the end face of the thrust bearing can be transformed from its annular (physical) domain to a rectangular (computational) domain. Accordingly, by substituting r=R exp(z/R) in equation (6), it is turned into the following form

$$\frac{1}{\gamma^2}\left[\nabla\bullet\left(\rho g\nabla p\right)\right]=\omega\frac{\partial}{\partial\vartheta}\left[\rho\left(H-f\right)\right]+\frac{\partial}{\partial t}\left(\rho H\right) \tag{7}$$

where $\nabla=\{\partial/(R\,\partial\vartheta),\ \partial/\partial z\}=\{\partial/\partial x,\ \partial/\partial z\}$ is the gradient operator and $\gamma=\gamma(z)=\exp(z/R)$ is the conformal mapping operator. In the computational domain $(\vartheta, z)$, for $\gamma=1$ equation (7) is the same as the thin film mechanics equation for journal bearings (eq. (5)). Hence equation (7) is the universal thin film mechanics equation for journal and thrust bearings, provided that $\gamma=1$ for journal bearings and $\gamma=\exp(z/R)$ for thrust bearings. If the fluid viscosity is considered constant across the film thickness and equal to the local mean viscosity (the one calculated at the cross-film averaged temperature), equations (2) can be easily integrated

$$\left.\begin{aligned} f&=H/2\\ g&=H^3/\left(12\mu\right)\end{aligned}\right\} \tag{8}$$

By means of substitution of eq. (8) into eq. (7), the universal Reynolds equation for journal and thrust bearings is obtained

$$\frac{1}{\gamma^2}\left[\nabla\bullet\left(\rho\frac{H^3}{12\mu}\nabla p\right)\right]=\frac{\omega}{2}\frac{\partial}{\partial\vartheta}\left(\rho H\right)+\frac{\partial}{\partial t}\left(\rho H\right) \tag{9}$$

### 3.2 Film thickness equations

As TEHD models take into account the deformations (due to both mechanical and thermal actions) of the two members of the pair, in order to calculate the film thickness H, the relative displacement of the two facing surfaces must be known.

Let $d_i$ be the displacement of a point on the surface i (i = 0, 1) in the normal direction (roughly the y direction for both the walls). Such a direction becomes radial in the case of a journal bearing, due to the curvature of the x axis. For very compliant bearings (i.e. for connecting rod applications) $d_i$ is the radial component of the displacement deprived of the rod rigid body motion, i.e., the mean displacement among points located on the sleeve surface. As explained in the previous paragraph, the reference frame is put on surface 0 and, precisely, in its real (deformed) configuration. This clarification implies that the equations of surface 0 and 1 can be expressed respectively by $H_0 = 0$ and $H_1 = H = h + d_1 - d_0$, where h is the ideal film thickness measured between the surfaces in undeformed state. The present paragraph deals with the assessment of the ideal film thickness h, while thermoelastic displacements $d_i$ are focused in paragraph 5.5.

Starting from a cylindrical (complete) journal bearing (Fig. 2) with no misalignment, the classical expression for the ideal film thickness, obtained by neglecting higher order infinitesimal terms, is $h= c_b + e \cdot \cos\theta$, where $c_b$ is the small radial clearance and e is the journal center eccentricity $O_bO_j$ (the norm of the vector **e**). As it evaluates h in the reference system O′(x′, y′) fixed to the center-line (the dash-dotted line in Fig. 2) that moves together with the journal, the above-mentioned classical expression is not suitable to deal with TEHD

analysis by means of FEM. Indeed, structural models can only evaluate the displacements of discrete points (nodes) on the bearing surface localized in a reference frame fixed to the bush. Hence the ideal film thickness equation must be also referred to a coordinate system fixed to the bearing, i.e. the reference frame O(x, y) shown in Fig. 2, by means of the following equation

$$h = c_b + e_X \cos\vartheta + e_Y \sin\vartheta \tag{10}$$

where the journal center location is given by the Cartesian coordinates ($e_X$, $e_Y$) in the reference frame $O_b(X, Y)$ fixed at the geometrical center of the shell.

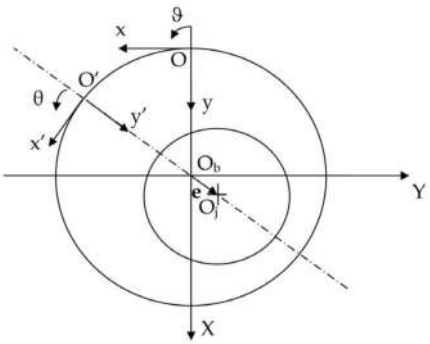


Fig. 2. Cylindrical pair (complete journal bearing) with ideal (rigid) members and reference systems

In a tilting pad thrust bearing assembly (Fig. 3), the geometrical center overlaps the origin of the reference system O(r, y, ϑ) used for the thin film mechanics equation (6). Hence O(X, Z) and its polar counterpart O(r, ϑ) are the references employed to measure the coordinates that rule the relative position of the assembly members. By moving their origin in the pivot

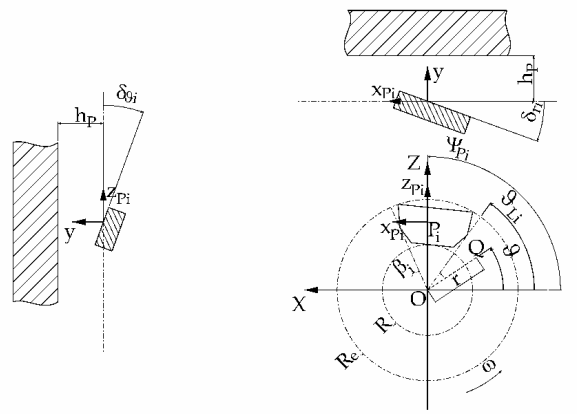


Fig. 3. Tilting pad-collar pair (thrust bearing) with ideal (rigid) members and reference systems

$P_i$ of the $i^{th}$ pad, the reference frame $P_i(x_{Pi}, z_{Pi})$ shown in Fig. 3 is obtained (the $z_{Pi}$ axis is oriented in radial direction), in order to easily express the ideal film thickness at pad i as

$$h_i = h_p - \delta_{ri} r \sin\left(\vartheta - \psi_{Pi}\right) + \delta_{\vartheta i}\left[r\cos\left(\vartheta - \psi_{Pi}\right) - r_{Pi}\right] \tag{11}$$

where the coordinate pair ($r_{Pi}$, $\psi_{Pi}$) gives the polar location of the pivot that supports the $i^{th}$ pad, $\delta_{ri}$ and $\delta_{\vartheta i}$ are the tilt angles of pad i around the radial axis $z_{Pi}$ and the tangential axis $x_{Pi}$ respectively (for line-contact pivots $\delta_{\vartheta i}$ =0), $h_P$ is the film thickness at pivot.
By substituting r = γ(z) R and/or ϑ = x/R in eqs. (10) and (11), the relevant ideal film thickness expressions in the mapped (computational) thin film domain O(x, z) are obtained.

### 3.3 Kinematic pairs motion equations

When the time history of the external load acting on the bearing is given instead of the relative position of the pair members, the resulting problem is referred to as *indirect problem* instead of *direct problem*. The indirect problem requires more relations than the sole thin film mechanics equation in order to determine the pressure field evolution, once the viscosity distribution is known by solving the energy equation. The additional relations are the equations of motion for the (moving) members of the kinematic pair.
One of the most effective iterative methods for solving the indirect problem (the coupled thin film mechanics and motion equations with the relevant initial and boundary conditions) is based on the Newton-Raphson procedure and it is explained, for different type of bearings, in many papers (i.e.: Chang et al., 2002).
Steadily loaded bearings are analyzed by means of the same method as dynamically loaded ones, whereas the mass-conserving approach (paragraph 4.1) retains the transient terms of eq. (7). In such a case, the simulated transitory evolving from an arbitrary initial condition is not meaningful, and only the steady conditions, reached after a sufficient number of time steps, are considered simulation results.
Unfortunately the resort to rotational equilibrium equations, which are simpler than momentum of momentum ones and might be sufficient to produce the fictitious transitory needed to reach the steady state, may cause the iterative procedure not to converge. Hence, rotational equilibrium equations are disregarded in the following and angular inertia is treated as a stabilization parameter for steady-state analyses.
Let **F** = {$F_X$, $F_Y$, 0} be the external load acting on the moving member of the pair.
In the case of a journal bearing (Fig. 2), the equilibrium equations of the journal are

$$\left.\begin{aligned} F_X + \int_\Omega p\cos\vartheta\,\gamma^2 d\Omega = 0 \\ F_Y + \int_\Omega p\sin\vartheta\,\gamma^2 d\Omega = 0 \end{aligned}\right\} \tag{12}$$

where Ω is the mapped domain (the union of the pad domains in a thrust bearing assembly) and $\gamma^2\, d\Omega = \gamma^2\, dx\, dz$ is an infinitesimal element of the physical domain. Equation (12) holds for steadily loaded and also dynamically loaded journal bearings, i.e. in a connecting rod big end bearing the inertia force acting on the journal is carried by the crankshaft bearing. In the case of a tilting pad thrust bearing (Fig. 3, $F_X$=0), the collar equilibrium implies

$$F_Y - \int_\Omega p\,\gamma^2 d\Omega = 0 \tag{13}$$

while the momentum of momentum equations for the (frictionless) $i^{th}$ pad motion are

$$\left.\begin{aligned} -\int_{\Omega} p\,\gamma\, R\sin\left(\vartheta-\psi_{Pi}\right)\gamma^2 d\Omega - I_{zPi}\frac{\delta_{ri}-2\delta_{ri}^{\,t-\Delta t}+\delta_{ri}^{\,t-2\Delta t}}{\Delta t^2}=0 \\ \int_{\Omega} p\left[\gamma\, R\cos\left(\vartheta-\psi_{Pi}\right)-r_{Pi}\right]\gamma^2 d\Omega - I_{xPi}\frac{\delta_{\vartheta i}-2\delta_{\vartheta i}^{\,t-\Delta t}+\delta_{\vartheta i}^{\,t-2\Delta t}}{\Delta t^2}=0 \end{aligned}\right\} \tag{14}$$

where $I_{xPi}$ and $I_{zPi}$ are the (mass) moment of inertia around the $x_{Pi}$ and $z_{Pi}$ axes, respectively, or the stabilization parameters of pad i.

## 4. The mass-conserving lubrication model

### 4.1 Integration domain and basic assumptions

Mass conserving cavitation models are based on the so-called JFO theory for moderately and highly loaded bearings, which assumes an infinite number of streamers in the cavitated region. Fig. 4 shows the thin film (mapped) computational domain Ω which is divided into an active (or pressurized) region $\Omega_a$ and an inactive (or cavitated) region $\Omega_c$ in such a way that $\Omega = \Omega_a \cup \Omega_c$. Let $\Gamma_e$ be the external boundary of Ω, $\Gamma_c$ the boundary between active and inactive film regions, $\Gamma_{e1}$ the eventual portion of $\Gamma_e$ that bounds the active film region and $\Gamma_{e2}$ the remaining part so that $\Gamma_e = \Gamma_{e1} \cup \Gamma_{e2}$. The unit vectors $\mathbf{n_a}$ and $\mathbf{n_c}$ denote the outwards normals respectively to $\Omega_a$ and $\Omega_c$.

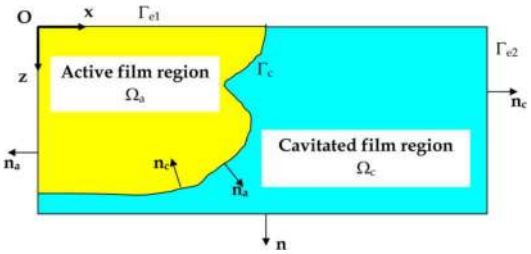


Fig. 4. Integration domain

It is assumed that the lubricant behaves like an incompressible fluid when hydrodynamic pressure build is allowed, and like a fictitious gas-liquid mixture with variable density and constant kinematic viscosity when cavitation occurs and pressure can be considered constant ($p = p_c$), so that mixture density ρ and viscosity μ are related to liquid density $\rho_L$ and viscosity $\mu_L$ by

$$\frac{\mu}{\mu_L}=\frac{\rho}{\rho_L} \tag{15}$$

The complete film region ($\rho = \rho_L$) includes $\Omega_a$ and in some cases, the part of $\Omega_c$ where pressure cannot rise and density is going to decrease, due to the divergence of the film, while the incomplete film region ($\rho < \rho_L$) is a portion of $\Omega_c$.

For the applications at the hand, the lubricant density $\rho_L$ is considered constant and the lubricant viscosity $\mu_L$ is assumed to depend solely on film temperature. In order to approximate the temperature-viscosity dependence of the lubricant in a range of

temperature that is quite narrow but still reasonable for steadily-loaded bearings, the following simple equation is often used

$$\mu_L = \mu_{L0} \exp\left[-\beta\left(T - T_0\right)\right] \tag{16}$$

where $\mu_{L0}$ is the lubricant viscosity at the reference temperature $T_0$ and $\beta$ a viscosity-temperature coefficient. By taking into account the assumptions about the lubricant behavior, the universal thin film mechanics equation (7) becomes

$$\Delta m = \frac{\rho_L}{\gamma^2}\left[\nabla\bullet\left(g_L \nabla p\right)\right] - \mathbf{U}\bullet\nabla\left[\rho\left(H - f_L\right)\right] - \frac{\partial}{\partial t}\left(\rho H\right) = 0 \tag{17}$$

where $\mathbf{U} = \{\omega R, 0\}$ is the relative velocity, $\Delta m$ the residual mass flow (per unit area) and

$$\left.\begin{aligned} f_L &= i_{L1} / i_{L0} = f \\ g_L &= i_{L2} - {i_{L1}}^2 / i_{L0} = g\ \rho/\rho_L \end{aligned}\right\} \tag{18}$$

with

$$i_{Ls} = \int_0^H \frac{y^s}{\mu_L}\, dy \tag{19}$$

Equation (17) ensures the continuity of the mass, by imposing that the difference between the lubricant flow into and out of the columnar element shown in Fig. 1 balances the variation of the mass per unit time in the same volume. The mass flow through the walls of the columnar element (per unit length) is

$$\mathbf{m} = -\frac{\rho_L\ g_L \nabla p}{\gamma} + \gamma\ \rho\left(H - f_L\right)\mathbf{U} \tag{20}$$

### 4.2 Classic Kumar and Booker type differential formulation

Assuming $\rho = \rho_L$ on region $\Omega_a$ and $p = p_c$ on region $\Omega_c$, the simulation of both the film regions may be performed by means of eq. (17), which becomes an elliptic equation in the unknown pressure p on $\Omega_a$ and a hyperbolic equation in the unknown density $\rho$ on $\Omega_c$. The method for determining the partitioning of region $\Omega$ takes advantage of a complementarity principle (Murty, 1974; LaBouff & Booker, 1985) that allows dividing the complete active from the complete inactive region, where pressure p and density derivative $\partial\rho/\partial t$ are calculated, respectively. Afterwards a time integration technique is used to compute the density $\rho$ of the film in such a way that the incomplete inactive region extent is immediately determined at each time step (Kumar & Booker, 1991).

### 4.3 Bonneau and Hajjam type differential formulation

An alternative formulation (Bonneau & Hajjam, 2001) turns out to be more accurate than the classic one in the case of dynamic loading conditions. In this approach the gas film content is defined as

$$\nu = -H\left(\rho_L - \rho\right) \tag{21}$$

Expressing the thin film mechanics equation (17) in terms of such variable yields

$$\Delta m = \frac{\rho_L}{\gamma^2}\nabla\bullet\left(g_L\nabla p\right) - \rho_L\mathbf{U}\bullet\nabla\left[H\left(1-\frac{f_L}{H}\right)\right] - \rho_L\frac{\partial H}{\partial t} - \mathbf{U}\bullet\nabla\left[\nu\left(1-\frac{f_L}{H}\right)\right] - \frac{\partial \nu}{\partial t} = 0 \tag{22}$$

Equation (22) must be integrated with the following constraints

$$\left.\begin{array}{l} \nu = 0 \quad and \quad p > p_c \quad on\ \Omega_a \\ p = p_c \quad and \quad \nu \le 0 \quad on\ \Omega_c \end{array}\right\} \tag{23}$$

that match the requirements of both regions $\Omega_a$ and $\Omega_c$ mentioned in the previous paragraph.

### 4.4 JFO cavitation conditions

The classic Jakobbson, Floberg and Olsson (JFO) conditions (Floberg & Jakobsson, 1957; Olsson, 1965) impose the continuity of the flow through the cavitation boundary $\Gamma_c$. They can be obtained by means of the flow balance suggested by Fig. 5, where $\mathbf{V_\Gamma}$ denotes the

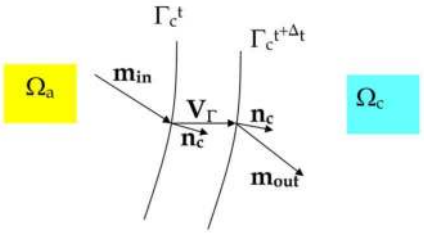


Fig. 5. Mass flows through the moving cavitation boundary

velocity of the moving boundary of $\Gamma_c$, crossed by the hydrodynamic mass flows $\mathbf{m_{in}}$ and $\mathbf{m_{out}}$, respectively leaving and entering the active film. Both such flows can be computed on the basis of eq. (20), particularized for $\Omega_a$ and $\Omega_c$. Therefore mass continuity through $\Gamma_c$ is ensured by the equation

$$\left.\begin{array}{l} \mathbf{m_{in}}\bullet\mathbf{n_c} - \mathbf{m_{out}}\bullet\mathbf{n_c} - H\left(\rho_L-\rho\right)\gamma\mathbf{V_\Gamma}\bullet\mathbf{n_c} = \\ = \left[\gamma\left(H-f_L\right)\left(\rho_L-\rho\right)\mathbf{U} - \frac{\rho_L\, g_L}{\gamma}\nabla p - \gamma\mathbf{V_\Gamma}H\left(\rho_L-\rho\right)\right]\bullet\mathbf{n_c} = 0 \end{array}\right\} \tag{24}$$

where all of the variables must be assessed on the boundary $\Gamma_c$. In this form, the JFO boundary conditions can be coupled with eq. (17) that is the Kumar and Booker's formulation.

In another way, in terms of the gas film content variable, by taking advantage of eq. (21), the same condition can be written

$$\left\{\gamma\nu\left[\left(1-\frac{f_L}{H}\right)\mathbf{U} - \mathbf{V_\Gamma}\right] + \frac{\rho_L g_L}{\gamma}\nabla p\bullet\mathbf{n_c}\right\} = 0 \tag{25}$$

which is the boundary condition on $\Gamma_c$ for the Bonneau and Hajjam's formulation of the mass conserving lubrication problem.

### 4.5 Strong differential hydrodynamic problem

The strong form of the differential problem is solved by finding the unknown pressure and gas content fields (respectively p and ν) that fulfill eq. (22) on Ω together with the relevant constraints eq. (23), the corresponding cavitation boundary conditions on $\Gamma_c$ (eq. (25)) and the essential boundary conditions $\nu = \nu_e$, $p = p_e$ on $\Gamma_e$.

### 4.6 Weak integral hydrodynamic problem

The film domain Ω is suitably discretized by a finite element mesh with n nodes. The differential equations must be turned into discrete systems of integral relationships employing the weighted residual method. Integration must be performed in the physical domain, which infinitesimal area is $\gamma^2\, d\Omega = \gamma^2\, dx\, dz$. Let $W_i$ be a weighting function associated with node i. After taking into account the different integration regions in Ω, the integral strong form of the problem can be expressed by the weighted equation

$$\left.\begin{aligned}
&\int_{\Omega_a} W_i \left\{ \frac{\rho_L}{\gamma^2} \nabla\bullet\left(g_L \nabla p\right) - \rho_L \mathbf{U}\bullet\nabla\left[ H\left(1-\frac{f_L}{H}\right)\right] - \rho_L \frac{\partial H}{\partial t} \right\} \gamma^2 d\Omega + \\
&+\int_{\Omega_c} W_i \left\{ -\rho_L \mathbf{U}\bullet\nabla\left[ H\left(1-\frac{f_L}{H}\right)\right] - \rho_L \frac{\partial H}{\partial t} - \mathbf{U}\bullet\nabla\left[ \nu\left(1-\frac{f_L}{H}\right)\right] - \frac{\partial \nu}{\partial t} \right\} \gamma^2 d\Omega + \\
&+\int_{\Gamma_c} W_i \left\{ \gamma\nu\left[\left(1-\frac{f_L}{H}\right)\mathbf{U} - \mathbf{V_\Gamma}\right] + \frac{\rho_L g_L}{\gamma}\nabla p \right\} \bullet \mathbf{n_c} \gamma\, d\Gamma
\end{aligned}\right\} \tag{26}$$

for i = 1 to n, together with the constraint eq. (23) and the essential boundary conditions on $\Gamma_e$. Applying the divergence theorem (eq. (A1), see appendix) and the Reynolds transport theorem (eq. (A2)) to the strong form (eq. (26)) yields

$$\left.\begin{aligned}
&-\rho_L \int_{\Omega_a} \nabla W_i \bullet g_L \nabla p\, d\Omega + \rho_L \int_{\Gamma_c \cup \Gamma_{e1}} W_i\, g_L \nabla p \bullet \mathbf{n_a}\, d\Gamma + \\
&+\rho_L \int_{\Omega_a} \nabla W_i \bullet H\left(1-\frac{f_L}{H}\right)\gamma^2 \mathbf{U}\, d\Omega - \rho_L \int_{\Gamma_c \cup \Gamma_{e1}} W_i H\left(1-\frac{f_L}{H}\right)\gamma^2 \mathbf{U}\bullet\mathbf{n_a}\, d\Gamma - \rho_L \int_{\Omega_a} W_i \frac{\partial H}{\partial t}\gamma^2 d\Omega + \\
&+\rho_L \int_{\Omega_c} \nabla W_i \bullet H\left(1-\frac{f_L}{H}\right)\gamma^2 \mathbf{U}\, d\Omega - \rho_L \int_{\Gamma_c \cup \Gamma_{e2}} W_i H\left(1-\frac{f_L}{H}\right)\gamma^2 \mathbf{U}\bullet\mathbf{n}_c\, d\Gamma - \rho_L \int_{\Omega_c} W_i \frac{\partial H}{\partial t}\gamma^2 d\Omega + \\
&+\int_{\Omega_c} \nabla W_i \bullet \nu\left(1-\frac{f_L}{H}\right)\gamma^2 \mathbf{U}\, d\Omega - \int_{\Gamma_c \cup \Gamma_{e2}} W_i \nu\left(1-\frac{f_L}{H}\right)\gamma^2 \mathbf{U}\bullet\mathbf{n}_c\, d\Gamma + \\
&-\frac{\partial}{\partial t}\int_{\Omega_c} W_i\, \gamma^2 \nu\, d\Omega + \int_{\Gamma_c \cup \Gamma_{e2}} W_i \gamma^2 \nu \mathbf{V_\Gamma}\bullet\mathbf{n}_c\, d\Gamma + \\
&+\rho_L \int_{\Gamma_c} W_i\, g_L \nabla p \bullet \mathbf{n_c} d\Gamma + \int_{\Gamma_c} W_i \gamma^2 \nu \left[\left(1-\frac{f_L}{H}\right)\mathbf{U} - \mathbf{V_\Gamma}\right] \bullet \mathbf{n_c} d\Gamma = 0
\end{aligned}\right\} \tag{27}$$

that considers the generic case shown in Fig. 4, where $\Omega_a$ is bounded by $\Gamma_c$ and a portion $\Gamma_{e1}$ of the external boundary. In such case the essential boundary conditions must be consistent, namely the gas film content has to vanish on $\Gamma_{e1}$. The relationship

$$\left.\begin{aligned}
&\mathbf{F}\bullet\mathbf{n_a} = -\mathbf{F}\bullet\mathbf{n_c} \quad on\ \Gamma_c \\
&\mathbf{n} = \mathbf{n_a} = \mathbf{n_c} \quad on\ \Gamma_e
\end{aligned}\right\} \tag{28}$$

holds for whatever field vector **F** is chosen, as evidenced by Fig. 4. Therefore, by taking into account eq. (28), equation (27) for $\Gamma_e = \Gamma_{e1} \cup \Gamma_{e2}$, $\Omega = \Omega_a \cup \Omega_c$ and $\nu = 0$ on $\Gamma_{e1}$, is turned into the relation

$$\left.\begin{aligned} &-\rho_L\int_\Omega \nabla W_i \bullet g_L \nabla p \, d\Omega + \rho_L \int_{\Gamma_e} W_i g_L \nabla p \bullet \mathbf{n} \, d\Gamma + \\ &+\rho_L\int_\Omega \nabla W_i \bullet H\left(1-\frac{f_L}{H}\right)\gamma^2 \mathbf{U} \, d\Omega - \rho_L \int_{\Gamma_e} W_i H\left(1-\frac{f_L}{H}\right)\gamma^2 \mathbf{U}\bullet\mathbf{n} \, d\Gamma - \rho_L \int_\Omega W_i \frac{\partial H}{\partial t}\gamma^2 \, d\Omega + \\ &+\int_\Omega \nabla W_i \bullet \nu\left(1-\frac{f_L}{H}\right)\gamma^2 \mathbf{U} \, d\Omega - \int_{\Gamma_e} W_i \gamma^2 \nu\left[\left(1-\frac{f_L}{H}\right)\mathbf{U} - \mathbf{V_\Gamma}\right]\bullet\mathbf{n} \, d\Gamma - \frac{\partial}{\partial t}\int_\Omega W_i \gamma^2 \nu \, d\Omega = 0 \end{aligned}\right\} \quad (29)$$

The lubricant flow, given by eq. (20), can be expressed in terms of the variable ν instead of ρ by means of eq. (21) as follows

$$\mathbf{m} = \gamma \, \rho_L H\left(1-\frac{f_L}{H}\right)\mathbf{U} + \gamma \, \nu\left(1-\frac{f_L}{H}\right)\mathbf{U} - \frac{\rho_L g_L}{\gamma}\nabla p \quad (30)$$

Then, by evidencing the expression of the flow (eq. (30)) and assuming that the external boundary is fixed with reference to surface 0 ($\mathbf{V_{\Gamma e}} = \mathbf{0}$), equation (29) becomes

$$\left.\begin{aligned} &\int_{\Gamma_e} W_i \mathbf{m}\bullet\mathbf{n} \, \gamma \, d\Gamma = -\rho_L \int_\Omega \nabla W_i \bullet \frac{g_L}{\gamma^2}\nabla p \, \gamma^2 d\Omega + \\ &+\rho_L\int_\Omega \nabla W_i \bullet H\left(1-\frac{f_L}{H}\right)\mathbf{U}\gamma^2 d\Omega - \rho_L \int_\Omega W_i \frac{\partial H}{\partial t}\gamma^2 d\Omega + \\ &+\int_\Omega \nabla W_i \bullet \nu\left(1-\frac{f_L}{H}\right)\mathbf{U}\gamma^2 d\Omega - \frac{\partial}{\partial t}\int_\Omega W_i \nu \gamma^2 d\Omega \end{aligned}\right\} \quad (31)$$

Equation (31) together with the constraint eq. (27) and the essential boundary conditions on $\Gamma_e$ completely defines the hydrodynamic problem in weak formulation. It allows to implicitly fulfill the continuity boundary conditions on $\Gamma_c$ (eq. (25)), which are embedded in Eq. (31) as just proved. The corresponding strong form of the problem is the Bonneau and Hajjam type differential formulation presented at paragraph 4.3.

By a numerical point of view the transient term in cavitated region can be evaluated as follows

$$\frac{\partial}{\partial t}\int_\Omega W_i \nu \gamma^2 d\Omega \cong \int_\Omega W_i \frac{\nu - \nu^{t-\Delta t}}{\Delta t}\gamma^2 d\Omega \cong \int_\Omega W_i \frac{\partial \nu}{\partial t}\gamma^2 d\Omega \quad (32)$$

where $\nu^{t-\Delta t}$ is the gas film content calculated at the previous time step.

Substitution of eqs. (32) and (21) in eq. (31) yields

$$\left.\begin{aligned} &\int_{\Gamma_e} W_i \mathbf{m}\bullet\mathbf{n} \, \gamma \, d\Gamma = -\rho_L \int_\Omega \nabla W_i \bullet \frac{g_L}{\gamma^2}\nabla p \, \gamma^2 d\Omega + \\ &+\int_\Omega \nabla W_i \bullet \rho\left(H - f_L\right)\mathbf{U}\gamma^2 d\Omega - \int_\Omega W_i \rho \frac{\partial H}{\partial t}\gamma^2 d\Omega - \int_\Omega W_i H \frac{\partial \rho}{\partial t}\gamma^2 d\Omega \end{aligned}\right\} \quad (33)$$

By means of eq. (33), which is roughly equivalent to eq. (31), the hydrodynamic problem is solved in the unknowns p, $\partial\rho/\partial t$ (instead of p, ν), as explained in paragraph 4.2. The corresponding strong form of the problem is the Kumar and Booker type differential formulation presented at paragraph 4.2.
Due to the different integration schemes, the two types of weak formulations are not numerically equivalent.

### 4.7 FEM formulation and stabilization

The weighting functions are usually chosen according to Galerkin method when elliptic problems are involved, i.e. $W_i = N_i$, where $N_i$ is the shape function of node i. The same expedient produces wiggles when the hyperbolic part of eq. (31) is solved in $\Omega_e$. Stabilization can be performed by means of the streamline upwind / Petrov-Galerkin (SUPG) method, which is element-independent and, in addition, sharply simplifies numerical implementation in comparison with the classical upwinding methods (Bathe, 1996).
In the present case, SUPG stabilization is achieved by adding numerical diffusion only along x direction. Hence, by introducing the usual finite element approximations for the unknown fields variables ($p = p_j N_j$ , $\nu = \nu_j N_j$), equation (31) can be written in synthetic form as

$$\Delta M_i = K^p{}_{ij}\, p_j + K^\nu{}_{ij}\, \nu_j + M^e{}_i + M^{t-\Delta t}{}_i = 0 \tag{34}$$

where

$$\left.\begin{aligned}
K^p{}_{ij} &= -\rho_L \int_\Omega \frac{g_L}{\gamma^2} \nabla N_i \bullet \nabla N_j \, \gamma^2 d\Omega \\
K^\nu{}_{ij} &= \int_\Omega \left[ \nabla N_i \bullet \left(1 - \frac{f_L}{H}\right) \mathbf{U} N_j - \frac{N_i N_j}{\Delta t} - \frac{\partial N_i}{\partial x} \tau^{SUPG} U^2 \left(1 - \frac{f_L}{H}\right)^2 \frac{\partial N_j}{\partial x} \right] \gamma^2 d\Omega \\
M^e{}_i &= \rho_L \int_\Omega \left[ \nabla N_i \bullet H \left(1 - \frac{f_L}{H}\right) \mathbf{U} - N_i \frac{H - H^{t-\Delta t}}{\Delta t} \right] \gamma^2 d\Omega \\
M^{t-\Delta t}{}_i &= \int_\Omega \frac{N_i}{\Delta t} \nu^{t-\Delta t} \gamma^2 d\Omega \\
\Delta M_i &= \int_{\Gamma_e} N_i \mathbf{m} \bullet \mathbf{n} \, \gamma \, d\Gamma
\end{aligned}\right\} \tag{35}$$

In eq. (35), Δt is the time step, $H^{t-\Delta t}$ and $\nu^{t-\Delta t}$ are respectively the film thickness and the gas film content calculated at the previous time, and $\tau^{SUPG}$ is the stabilization parameter

$$\tau^{SUPG} = \alpha^{up} \beta^{up} \frac{\Delta s}{|\mathbf{u_s}|} \tag{36}$$

where $\alpha^{up}$, $\beta^{up}$ are dimensionless coefficients used to control the added diffusion, Δs is the length of the finite element along the streamwise direction, and $\mathbf{u_s}$ the convective flow velocity. In eq. (36) the term on the right hand side has the effect of weighting the convection operators towards the upstream direction.

In order to solve eq. (34), the following set of values is used in eq. (36): $\alpha^{up} = 1$, $\beta^{up} = 0.5$, $\Delta s = \Delta x$ (element length along the x direction) and $u_s \approx U / 2$, whereas the convective flow in the cavitated region moves in x direction with the mean surface velocity.
Some authors (Fatu et al., 2006) assume that viscosity is independent of cross film direction y in the cavitated region so that $f_I/H = 0.5$ in $\Omega_c$.

## 5. Fast energy-conserving thermal models

### 5.1 2D model

A simplified energy conservation equation for thin fluid films was derived by averaging in the cross-film direction the classic 3D energy equation (Kumar & Booker, 1994). Although the resulting 2D model is very fast by a computational point of view, it is unable to assess the temperature gradient $\partial T/\partial y$ at the walls, which must be considered adiabatic. By applying the conformal mapping defined in paragraph 3.1, the 2D energy equation is turned into the following relation

$$\Delta q = \frac{1}{\gamma^2}\nabla\bullet\left(K\,H\,\nabla T_m\right) - \rho\frac{c}{\gamma}H\,\mathbf{u_m}\bullet\nabla T_m - \rho c\,H\frac{\partial T_m}{\partial t} + H\Phi_m = 0 \tag{37}$$

where the subscript m denotes a variable averaged in the transverse direction of the film y, $\Delta q$ the residual heat flow (per unit area), $\mathbf{u} = \{u, v, w\}$ the lubricant velocity vector, K the thermal conductivity of the lubricant film mixture, c the specific heat and $\Phi$ the power dissipation density function.
Equation (37) ensures the continuity of the energy, by imposing that the net heat exchanged by the columnar element of fluid shown in Fig. 1 balances the variation of internal energy and the heat dissipation in the same volume. The heat flow through the walls of the columnar element is

$$\mathbf{q} = -\frac{H}{\gamma}K\nabla T_m \tag{38}$$

The conduction in the oil film plane (x, z) is not taken into account in the original equation devised by Kumar & Booker, as the problem solution is dominated by convection. The conductive term has been introduced in eq. (37) only for numerical convenience, in order to take advantage of SUPG stabilization (paragraph 5.3).

### 5.2 Quasi-3D model

Equation (37) can be modified in order to take into account the heat flux from the lubricant film into the two members of the pair. In this case, the heat absorbed by the film is equal to the difference between the viscous dissipation and the total heat exchange.
Therefore, the following equation is used in the thin film region $\Omega$

$$\Delta q = \frac{1}{\gamma^2}\nabla\bullet\left(K\,H\,\nabla T_m\right) - \rho\frac{c}{\gamma}H\,\mathbf{u_m}\bullet\nabla T_m - \rho c\,H\frac{\partial T_m}{\partial t} + H\Phi_m - q_0 - q_1 = 0 \tag{39}$$

where $q_0$ and $q_1$ are the heat transfers (per unit area) to surface 0 and 1, respectively.
They are calculated by obtaining the temperature gradients at the walls, in the hypothesis that the temperature profile across the film thickness is a fourth-order polynomial.

According to the procedure explained in detail in the previous reference work (Stefani & Rebora, 2009), the five coefficients of this polynomial can be calculated by:
a) equating the film temperature at the walls with the temperatures $T_0$ and $T_1$ calculated by the heat conduction equations on surface 0 and 1 respectively; b) imposing that the average temperature in the y direction is equal to $T_m$, namely the unknown of eq. (39). The resulting heat exchange at the wall surfaces is

$$\left.\begin{aligned} q_0 &= K\left.\frac{\partial T}{\partial y}\right|_{y=0} = \frac{K}{H}\left(5T_m - \frac{7}{2}T_0 - \frac{3}{2}T_1 - \frac{1}{8}T_0''H^2 + \frac{1}{24}T_1''H^2\right) \\ q_1 &= K\left.\frac{\partial T}{\partial y}\right|_{y=H} = \frac{K}{H}\left(5T_m - \frac{3}{2}T_0 - \frac{7}{2}T_1 + \frac{1}{24}T_0''H^2 - \frac{1}{8}T_1''H^2\right) \end{aligned}\right\} \tag{40}$$

where $T''_0$ and $T''_1$ are the derivatives $\partial^2T/\partial y^2$ at the surfaces 0 and 1, respectively.
They can be obtained by projecting the 3D energy equation on both the kinematic pair surfaces. Particularly in steady-state conditions ($\partial T/\partial t=0$, $\partial H/\partial t=0$), under the further assumptions that the temperature on surface 1 does not depend on the x coordinate ($\partial T_1/\partial x=0$), evaluating the 3D energy equation on surfaces 0 and 1 yields respectively

$$\left.\begin{aligned} T_0'' &= \left.\frac{\partial^2 T}{\partial y^2}\right|_{y=0} = -\frac{1}{K}\Phi(x,0,z) = -\frac{\Phi_0}{K} \\ T_1'' &= \left.\frac{\partial^2 T}{\partial y^2}\right|_{y=H} = -\frac{1}{K}\Phi(x,H,z) = -\frac{\Phi_1}{K} \end{aligned}\right\} \tag{41}$$

The hypothesis $\partial T/\partial x=0$ on surface 1 is extensively adopted in the analysis of journal bearings, where the shaft rotation flattens the circumferential variations of temperature (Kucinski et al., 2000). An analogous phenomenon may occur in thrust bearings due to the collar rotation.
The hypothesis $\partial T/\partial t=0$ complies with the analysis of steadily loaded bearings. It is also sufficiently realistic in the simulation of dynamically loaded bearings, as the variations of temperature distribution in the bearing structure over one load cycle are not very significant in comparison with film temperature changes (Kim & Kim, 2001). Nevertheless, equation (41) does not take into account the heat convection due to squeeze and it must be modified to deal with dynamic loading conditions. In addition a full transient thermal analysis ($\partial T/\partial t\neq 0$) requires special techniques (Fatu et al., 2006).
Equation (41) implicitly includes the velocity boundary conditions $\mathbf{u} = 0$ for y = 0 as well as $v = \gamma U\, dH/dx$, w=0 for y = H, so that the derivatives $T''_0$, $T''_1$ become independent of heat convection. Such a deduction, proved in the previous reference work (Stefani & Rebora, 2009) dealing with journal bearings, has been extended to thrust bearings by taking advantage of the reference system choice (paragraph 3.1).

### 5.3 FEM formulation and stabilization

The following SUPG-stabilized integral form of eq. (39) (and eq. (37) as particular case) is here proposed

$$\Delta Q_i = K^T{}_{ij}\, T_{mj} + Q^{\Phi}{}_i + Q^{t-\Delta t}{}_i - Q^0{}_i - Q^1{}_i = 0 \tag{42}$$

where

$$\left.\begin{aligned}
K^T{}_{ij} &= -\int_{\Omega}\left(\frac{1}{\gamma^2}\nabla N_i\,\mathbf{K}\nabla N_j + N_i\frac{\rho c}{\gamma}H\,\mathbf{u_m}\bullet\nabla N_j + \rho c\,H\frac{N_i N_j}{\Delta t}\right)\gamma^2 d\Omega \\
Q^{\Phi}{}_i &= \int_{\Omega} N_i H\,\Phi_m\,\gamma^2 d\Omega \\
Q^{t-\Delta t}{}_i &= \int_{\Omega}\rho c\,H\frac{N_i}{\Delta t}T_m{}^{t-\Delta t}\,\gamma^2 d\Omega \\
\Delta Q_i &= -\int_{\Gamma e} N_i H\,K\nabla T_m\bullet\mathbf{n}\,d\Gamma = \int_{\Gamma e} N_i\mathbf{q}\bullet\mathbf{n}\,\gamma\,d\Gamma \\
Q^0{}_i &= \int_{\Omega} N_i q_0\,\gamma^2 d\Omega \\
Q^1{}_i &= \int_{\Omega} N_i q_1\,\gamma^2 d\Omega
\end{aligned}\right\} \tag{43}$$

In eq. (43) $T_m{}^{t-\Delta t}$ is the (averaged) film temperature calculated at the previous time and **K** is the following diffusivity matrix

$$\mathbf{K} = \begin{bmatrix} KH + cC\,\tau^{SUPG}u_m{}^2 & cC\,\tau^{SUPG}u_m w_m \\ cC\,\tau^{SUPG}w_m u_m & KH + cC\,\tau^{SUPG}w_m{}^2 \end{bmatrix} \tag{44}$$

where C is a reference clearance value. Specifically $C=c_b$ for complete cylindrical journal bearings (eq. (10)) and $C = h_P{}^{ref}$ (reference film thickness at pivots) for thrust bearing assemblies (eq. (11)). As in the last case the film thickness at pivot $h_P$ is a variable and a fixed parameter for all the time steps is required in the stabilization procedure, a suitable reference thickness at pivot $h_P{}^{ref}$ is chosen (i.e. for most thrust bearings a good value of $h_P{}^{ref}$ is 50 μm).
In order to avoid wiggles in the temperature distributions retrieved from eq. (42), the $\tau^{SUPG}$ stabilizing parameter is calculated by means of eq. (36), with $\alpha^{up}=1$, $\beta^{up}=0.5$, and $u_s=|\mathbf{u_m}|$.

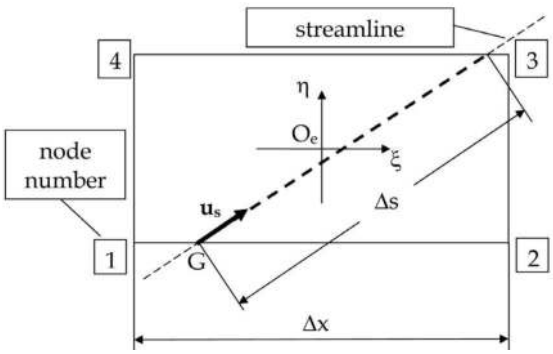


Fig. 6. Streamline across a 4-node isoparametric finite element, where $O_e(\xi, \eta)$ is the element reference system and G is a Gauss point

As the integrals in eq. (43) are evaluated by means of the 2-points Gauss quadrature, the length $\Delta s$ in eq. (36) is calculated along the streamline across every Gauss point G, as shown in Fig. 6. Since convection typically dominates diffusion along the flow direction, the added streamwise diffusion does not compromise the accuracy of the solution in this direction. In addition no deleterious cross-stream diffusion is added.

### 5.4 FEM groove mixing theory

If the region $\Omega_g$ is the projection in the (x, z) plane of the $g^{th}$ groove fed with supply oil at temperature $T_s$, the average film temperatures $T_{m\Omega g}$ and $T_{m\Gamma g}$ are assumed to be uniform throughout $\Omega_g$ and its boundary $\Gamma_g$, respectively. The proposed algorithm is based on the simple idea that the residuals of the integral energy equations calculated at nodes belonging to the grooves must be involved in the calculation. This enables us to assess the entry temperature, which experimental evidence suggests is higher than the oil-feed temperature. An approximated energy balance provides the additional equation needed to evaluate the unknown entry temperature $T_{m\Gamma g}$.

$N_i$ being the $i^{th}$ shape function, n the number of the nodes in $\Omega$, $n_g$ the number of the nodes in $\Omega_g$, and $n_{bg}$ the number of nodes lying on the groove boundary $\Gamma_g$, the energy-balance equation for the oil flows that mix in $\Gamma_g$ is given by

$$\begin{aligned} &\sum_{i=1}^{ng}\int_{\Omega g} N_i \Delta q_g \gamma^2 d\Omega + \sum_{i=1}^{n}\int_{\Gamma g} N_i \mathbf{q}\bullet\mathbf{n}\gamma d\Gamma + c\int_{\Gamma g} N_i \mathbf{m}\bullet\mathbf{n}\gamma d\Gamma\left(T_{m\Gamma g} - T_s\right) = \\ &= \sum_{i=1}^{nbg} \Delta Q_i^{\,g} + \Delta Q_i + c\,\Delta M_i\left(T_{m\Gamma g} - T_s\right) = 0 \end{aligned} \tag{45}$$

where $\Delta q_g$ and $\Delta Q_i{}^g$ are the local and the integral residual at node i, respectively, of the energy balance in the groove domain $\Omega_g$, described below. In eq. (45) $\Delta Q_i$ and $\Delta M_i$ are the weighted residual (calculated at node i) of the energy and thin film mechanics equations integrated in $\Omega$ according to eqs. (42) and (34), respectively. $\Omega_g$ is not a thin film region and therefore it is *not* a part of the integration domain $\Omega$. Hence in $\Omega_g$ the specific energy balance equation at node i is required to conserve energy and to determine $T_{m\Omega g}$

$$\Delta Q_i^{\,g} = \int_{\Omega g} N_i \Delta q_g \gamma^2 d\Omega = 0 \tag{46}$$

In eq. (46) $\Delta q_g$ evaluates the net heat flow in the region $\Omega_g$, calculated by

$$\Delta q_g = \Phi_{gm} H_g - 2\alpha_0 q_{0g} - q_{1g} \tag{47}$$

where $H_g$ is a groove equivalent thickness, $\Phi_g$ is the groove power dissipation density function, $\alpha_0$ is the ratio between the effective conductive area of the grooves (lying on surface 0) and their total area projected on surface 0 and 1, and $q_{0g}$, $q_{1g}$ are the heat flows exchanged with the surface 0 and 1, respectively, in the region $\Omega_g$; $q_{0g}$ and $q_{1g}$ are given by

$$\left.\begin{aligned} q_{0g} &= K\left.\frac{\partial T}{\partial y}\right|_{y=0} = \frac{K}{H_g}\left(5T_{m\Omega g} - \frac{7}{2}T_0 - \frac{3}{2}T_1 + \frac{1}{8}\frac{\Phi_{g0}}{K}H_g{}^2 - \frac{1}{24}\frac{\Phi_{g1}}{K}H_g{}^2\right) \\ q_{1g} &= K\left.\frac{\partial T}{\partial y}\right|_{y=Hg} = \frac{K}{H_g}\left(5T_{m\Omega g} - \frac{3}{2}T_0 - \frac{7}{2}T_1 - \frac{1}{24}\frac{\Phi_{g0}}{K}H_g{}^2 + \frac{1}{8}\frac{\Phi_{g1}}{K}H_g{}^2\right) \end{aligned}\right\} \tag{48}$$

Equation (48) has been obtained by combining eqs. (40) and (41). Hence, eq. (48) does not hold for a thick film in a general case, but remains valid if the groove hydrodynamic behavior is simulated as an equivalent Couette flow (in laminar regime with negligible body forces) into a gap of uniform thickness $H_g$ with each wall at uniform temperature. In this hypothesis, if the relevant shear stress is denoted by $\tau_g$, the groove power dissipation density function $\Phi_g$ at the walls and its mean value $\Phi_{gm}$ are given by

$$\Delta q_g = \Phi_{g0} = \Phi_{g1} = \Phi_{gm} = \tau_g \frac{U}{H_g} = \frac{1}{2}\frac{\lambda \rho U^3}{H_g} \tag{49}$$

where the friction factor $\lambda$ characteristic of the groove type, is defined by

$$\lambda = \frac{\tau_g}{\frac{1}{2}\rho U^2} \tag{50}$$

Application of the FEM groove mixing approach to the study of different types of grooves is made possible by means of a reasonable choice of the characteristic parameters $\lambda$ and $H_g$. The Wendt (Wendt, 1933) and the surface drag losses (Khonsari & Booser, 2008) empirical formulas have been used to assess the friction factor $\lambda$ for journal and thrust bearings, respectively.

### 5.5 Structural and thermal simulation of the pairs

Steady-state elasticity and heat conduction equations must be solved in the structures of the kinematic pair members to assess the displacements due to mechanical as well as thermal actions and the temperature of the bearing surfaces due to heat dissipation in the lubricant film. By taking advantage of the related problem linearity as well as of FEM condensation procedures, the thermoelastic displacements $d_i$ and the thermal fields $T_i$ of the two surfaces (i=0, 1) are obtained by means of linear operators, which numerical counterparts are represented by suitable vectors and matrices. They may be calculated in a preprocessing phase, by means of a separate (commercial) FEM code, i.e. Ansys, which is very flexible and suitable to perform complex operations thanks to the APDL language.

The displacements due to mechanical actions $d^m_i$ and due to thermal dilatation $d^t_i$ are evaluated separately, so that $d_i = d^m_i + d^t_i$.

In order to compute mechanical displacements $d^m_i$ (in the y direction) of the two surfaces (i=0, 1), the following linear expression is used

$$d^m{}_i = d^{me}{}_i + C^m{}_i A p \tag{51}$$

where $d^{me}_i$ is the additional displacement due to external mechanical actions, $C^m_i$ is the compliance operator of the structure and A is a suitable area operator.

A typical external action is the bolt preload in connecting rod journal bearings, which leads to the $d^{me}_i$ contribution. For journal bearings the displacement direction is radial and the mean displacement of the bearing surface must be subtracted (paragraph 3.2). The assumption $d^m_1 = 0$ is very usual for both journal and thrust bearings, as shaft and collar are much stiffer than bush and pads. Details about the calculation procedure can be found in many papers (i.e.: Bonneau & Hajjam, 2001).

In order to compute the thermal field $T_i$ on the two surfaces (i=0, 1), the linear equation is

$$T_i - T_e = T^e{}_i + S_i A q_i \tag{52}$$

where $T_e$ is the external temperature, $T^e{}_i$ is the temperature field due to essential boundary conditions on a part of the thermal model, and $S_i$ is referred to as thermal sensitivity operator. $T_e$ is the bulk temperature of the air surrounding the structure, whereas heat convection boundary conditions are used to model the heat exchange with the environment. Essential boundary conditions on the groove surface ($T_0=T_s$ on $\Omega_g$) may be useful in order to simulate the heat exchange between cold lubricant and hot metal, which is influential when $T_s$ value is not much higher than $T_e$. In such a case $T^e{}_i$ must be computed, unless the temperature $T_e$ and $T_s$ are assumed to be equal as in the plain bearing studied in the reference work (Stefani & Rebora, 2009). The same paper deals with the procedure required to calculate the tensors for the discretization of eq. (52), except $T^e{}_i$.
In order to compute thermal displacements $d^t{}_i$ (in the y direction) of the two surfaces (i=0, 1), the linear expression is

$$d^t{}_i = d^{te}{}_i + C^t{}_i A q_i \tag{53}$$

where $d^{te}{}_i$ is the additional displacement due to essential temperature boundary conditions, $C^t{}_i$ is the thermal compliance operator. In eq. (53) $d^{te}{}_i$ is the displacement due to the temperature field $T^e{}_i$ discussed above. The assessment of $C^t{}_i$ is discussed in the above-cited reference work, where it is expressed as the product of two tensors, evaluated in separate thermal and structural analyses. Indeed $C^t{}_i$ may be also estimated directly by resorting to coupled-field solid elements.

## 6. Application examples

### 6.1 Journal bearing

In order to show the degree of reliability of the above-explained methods, a comparison among experimental and numerical results is presented for the two-axially grooved journal bearing studied by Lund (Lund & Tonnesen, 1984). Extensive bibliography, simulation details, assumed bearing data and boundary conditions are reported in the reference work (Stefani & Rebora, 2009). Fig. 7 shows the trends of the temperature $T_0$ (on the bush surface) along the bearing centerline for a shaft rotation speed of 5000 rpm and an external load of 5600 N. The responses of the 2D THD model and the quasi-3D TEHD model (with $\alpha_0=5$ in eq. (47)) are compared.
Particularly, the 2D model (dotted line) strongly underestimates the experimental temperature, as explained in the reference work. The dash-dotted line is obtained by assuming, in agreement with the reference and the Lund's work, that the temperature of the effective area 2 $\alpha_0$ $\Omega_g$ exchanging heat with the oil film is constant and equal to the supply oil temperature $T_s$ (hypothesis A). Such an assumption means that $T_0=T_s$ is imposed in eq. (48), but the groove surface temperature in the thermal model is free ($T^e{}_0=0$ in eq. (52)), so that the dash-dotted line exceeds Ts=50°C in the groove regions (85°≤ϑ≤95° and 265°≤ϑ≤275°) in Fig. 7. Although such response seems to be realistic by the physical point of view, as a limited variation of the white metal temperature through the groove region is expected, the hypothesis A requires different assumptions in different sub-models. Differently the solid line has been obtained by imposing $T_0=T_s$ in $\Omega_g$ coherently in all of the sub-models (hypothesis B). In the present bearing study, the supply temperature is greater than the

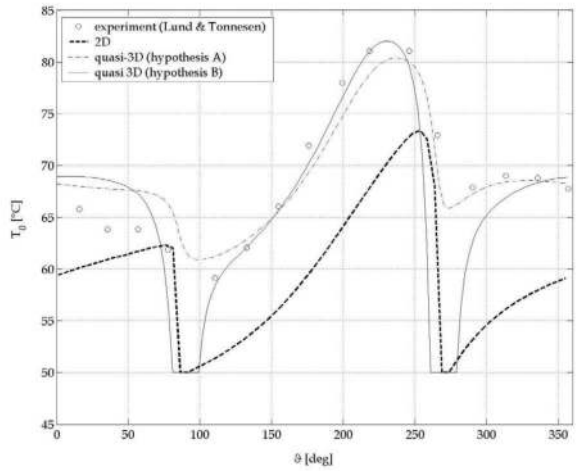


Fig. 7. Centerline temperatures on the bearing surface calculated by means of the 2D model and the quasi-3D model (two-axial groove journal bearing, ω=5000 rpm, $F_X$=5600 N)

external temperature ($T_s$=50°C, $T_e$=20°C) and, therefore, the thermal simulation requires the calculation of the term $T^e_0$ in eq. (52) in order to fulfil hypothesis B. Accordingly $T_0=T_e$ has been imposed on $\Omega_g$ while calculating the corresponding sensitivity matrix (term $S_0$ in eq. (52)).
The adoption of either hypothesis A or B enables the heat exchange between the structure of the bush and the lubricant in the grooves to be simulated. The lack of such modelling detail causes, in the present case, a bush peak temperature overestimation of roughly 10°C. Although hypothesis A yields a better temperature trend than hypothesis B, it leads to an underestimation of the journal temperature that is evident in the cited Lund's paper too. A comparison among journal temperature results is reported in Table 1, where axially averaged values are calculated for the one-dimensional journal sub-models adopted in the quasi-3d analyses (see the reference paper for details).

| | Experiment (Lund & Tonnesen) | Quasi-3D (hypothesis B) | Quasi-3D (hypothesis A) | Lund calculation |
|---|---|---|---|---|
| $T_1$ [°C] | 77.8 | 78.7 | 74.5 | 73.1 |

Table 1. Journal temperatures: experimental vs. numerical results (average values)

### 6.2 Thrust bearing

Another comparison among experimental and numerical results is presented for the tilting-pad thrust bearing studied by Glavatskikh, who published accurate experimental results (Glavatskikh, 2001). This publication also furnishes the bearing data needed by the analyses. The thermal and the thermoelastic behavior of the thrust bearing is taken into account (in the quasi-3D analysis) by means of a 3D model of the pad and 2D axisymmetric model of the shaft-collar assembly (Fig. 8). The choice of an axisymmetric collar model complies with the assumption $\partial T_1/\partial x=0$ (paragraph 5.2).

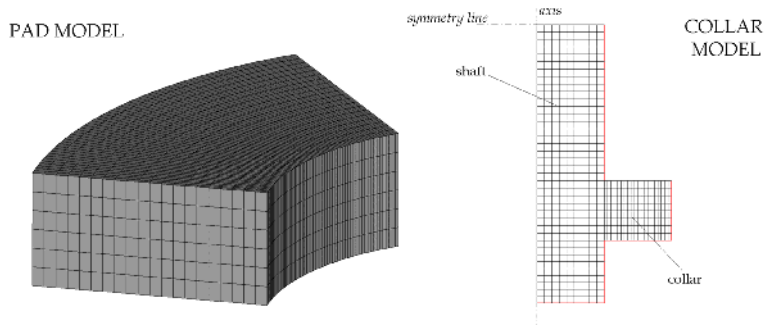


Fig. 8. Finite element models of the thrust pads and the shaft-collar assembly

In the pad thermal and thermoelastic models, used to calculate the thermal sensitivity $S_0$ (eq. (52)) and the thermal compliance $C^t_0$ (eq. (53)) respectively, convective heat transfer boundary conditions are assumed for all of the thrust pad surfaces except the babbitt face (surface 0) where the nodal heat flows are applied.

Analogous temperature boundary conditions are adopted for the collar (in Fig. 8 the red lines locate the convective surfaces) and, in addition, symmetry (natural) boundary conditions are reasonably assumed in order to model only a quarter of the shaft, as the test rig is made by two opposite thrust bearings. The heat transfer coefficient and the bulk temperature are set to 50 W $m^{-2}$ $°C^{-1}$ and 20°C, respectively, for all of the pad and shaft-collar convective surfaces.

Different displacement boundary conditions are imposed in the assessment of the thermal compliance $C^t_i$ and the structural compliance $C^m_i$ (eqs. (53) and (51), respectively).

In the former case, the outer surfaces of both the thrust pad and the shaft-collar assembly are left free to expand and only the in-plane displacements of a suitable number[1] of nodes lying on these surfaces have been constrained to avoid ill-conditioning. In the latter case, a small portion of the pad bottom surface around the pivot has been constrained from moving and, in addition, the radial displacements of all of the pad nodes located on the outer and inner diameters are constrained. The collar is assumed to be much stiffer than the pad ($C^m_1=0$) and for both the pads and the collar no external mechanical action is considered ($d^{me}_0=d^{me}_1=0$ in eq. (51)). The shaft-collar symmetry constraint is enforced in the thermoelastic model by locking the axial displacement of all of the nodes lying on the symmetry line (Fig. 8).

As the metal on the bottom of the groove cavity (the carrier ring) is not simulated, the lubricant in the inner groove region is assumed to remain, on the average, at the supply oil temperature ($T_{m\Omega g}=T_s$), while the groove boundary mean temperature $T_{m\Gamma g}$ is still an unknown of the problem. Consequently, no essential temperature boundary conditions on the groove surface $\Omega_g$ are required on both thermal and thermoelastic models ($T^e_i=d^{te}_i=0$ in eqs. (52) and (53)).

The universal Reynolds equation (eq. (9)) has been used to obtain the results reported below for 1 MPa specific load ($F_Z$=26130 N) and $T_s$=40°C supply temperature. Radial tilt of pads is neglected ($\delta_{\vartheta i}=0$). For the quasi-3D model, the coefficient $\alpha_0$ (eq. (47)) is increased from 0 to 5 when the rotation speed decreases from 3000 rpm to 1500 rpm, as the heat transfer in the

[1] 4 nodes for the pad 3D model, 3 nodes for the shaft-collar 2D model

grooves is more efficient at low speed, when the lubricant flow rate entering the fully flooded pad inlet is low in comparison with the (constant) flow rate supplied to the test rig.
Fig. 9 shows the variation with the shaft rotation speed of the pad (surface 0) temperature $T_{75/75}$, assessed at a location $r_{75}$=R+0.75 ($R_e$-R), $\vartheta_{75}=\vartheta_{Li}+0.75\beta_i$ (Fig. 3), of the collar (surface 1) temperature $T_{75}$ at the location r=$r_{75}$, and of the shaft temperature $T_s$ at the location r=0 (on the pivot plane). For the 2D model, which does not evaluate wall temperatures, only the mean film temperature at the point ($r_{75}$, $\vartheta_{75}$) is reported in Fig. 9. Again, in comparison with the reference experimental results, the 2D model strongly underestimates the temperatures, while the quasi-3D model ensures a good level of reliability. In the same Fig. 9 the calculated oil flow rate M is also given. The oil flow rate supplied to the test rig is 15 l/min. Excess flow, beyond what is needed hydrodynamically, acts to provide overall cooling to the bearing. Therefore the assumed variation of $\alpha_0$ with the rotation speed is well-justified.

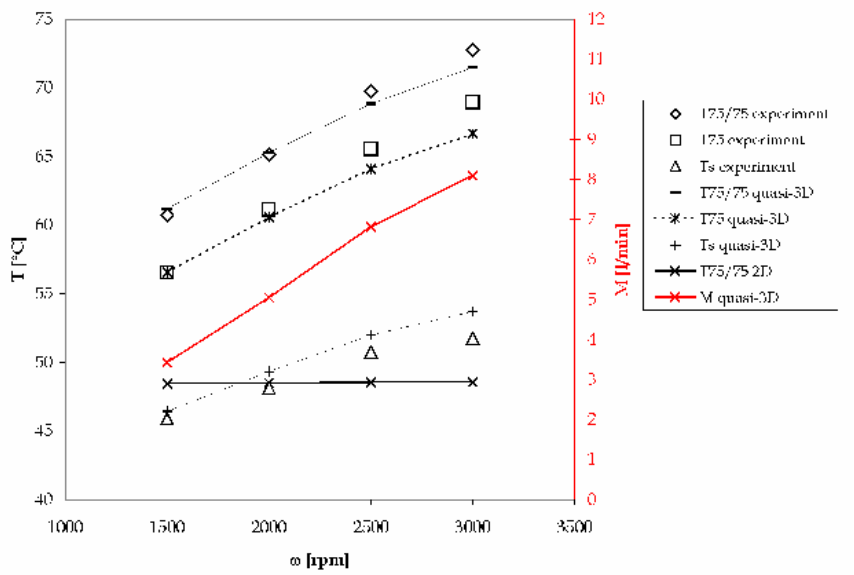


Fig. 9. Pad ($T_{75/75}$), collar ($T_{75}$), shaft ($T_s$) temperature and calculated flow rate (M)

The corresponding variations of the power loss P and of the film thickness at the pad inlet and outlet ($h_1$ and $h_3$, respectively) are given in Fig. 10. The temperature underestimation of the 2D model leads to unreliable predictions of the film thickness.
Fig. 11 a) compares the experimental and theoretical (quasi-3D model) circumferential variations of pressure $p_{25}$ and $p_{75}$ evaluated at $r_{25}$ and $r_{75}$, respectively, for ω=3000 rpm. By removing the constraint $\delta_{\vartheta i}$=0, the differences between theoretical and experimental peak pressures increase. For the same rotation speed, Fig. 11 b) shows the pressure distribution calculated by means of the quasi-3D model on the 6 pads of the bearing. The maximum value of this distribution is 2.4 MPa, which is very close to the peak of the experimental pressure $p_{75}$ (2.3 MPa).
The overall agreement between numerical and experimental results might be further improved by taking into account the variation of the viscosity across the film thickness.

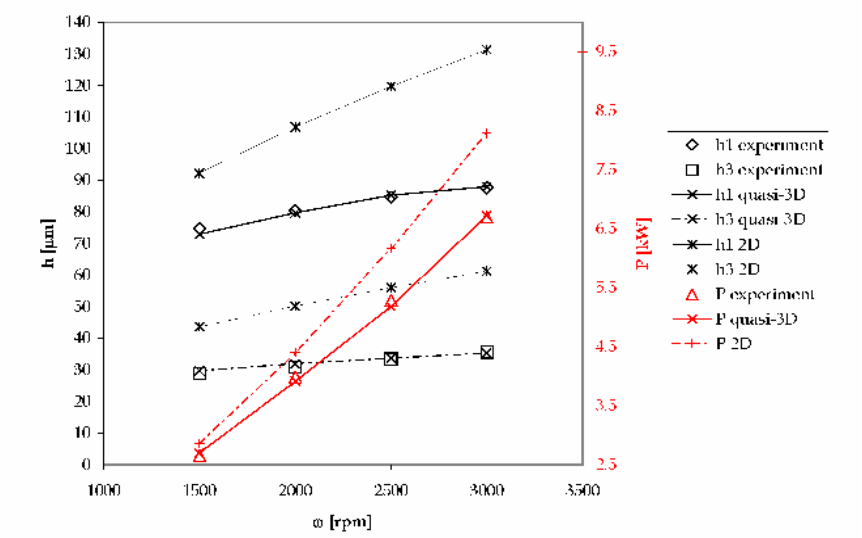


Fig. 10. Power loss (P) and film thickness at pad inlet ($h_1$) and outlet ($h_3$)

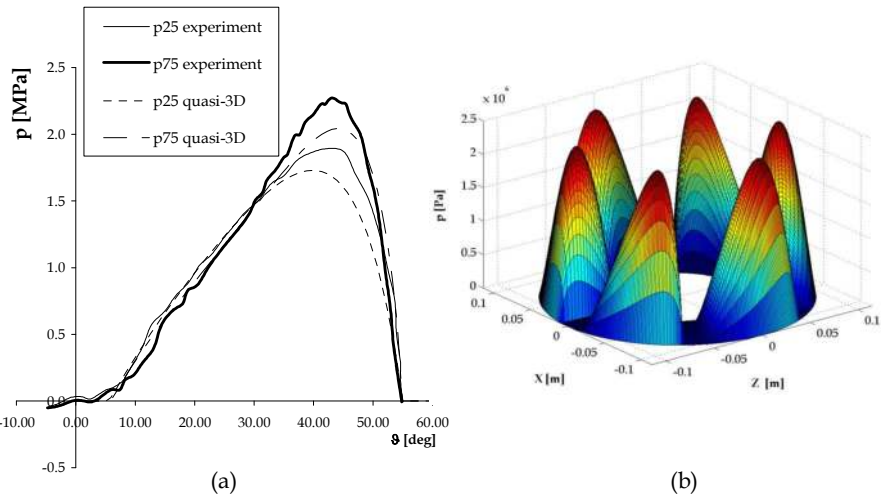


Fig. 11. Hydrodynamic pressure for ω=3000 rpm: a) circumferential variations ($p_{25}$, $p_{75}$); b) pressure field computed by means of the quasi-3D model

## 7. Conclusion

A general-purpose FEM approach to the TEHD analysis of hydrodynamic bearings has been described, focusing on the theoretical aspects, whereas the relevant numerical procedures are reported in a large number of papers. Particularly, the most used FEM formulations of

the mass-conserving lubrication problem have been proved, while an original approach to the thermal problem has been explained.
The numerical examples show how the quasi-3D approach has enhanced the reliability of the mass- and energy-conserving lubrication analysis proposed by Kumar and Booker.
Indeed, TEHD models are very sensitive to boundary conditions, which choice is particularly difficult in all of the multi-physics simulations.
Future work will adapt the devised method to detailed transient analyses and it will further extend the model flexibility by including advanced turbulent lubrication theory.

## 8. Appendix

Let f and **F** be scalar and vector-valued functions respectively. A variant of the divergence theorem states

$$\int_{\Omega}\left(\mathbf{F}\bullet\nabla f + f\,\nabla\bullet\mathbf{F}\right)d\Omega = \int_{\Gamma} f\,\mathbf{F}\bullet\mathbf{n}\;d\Gamma \tag{A1}$$

where Γ is the boundary of Ω oriented by the outward-pointing unit normal **n**.
If $\mathbf{V}_{\Gamma}$ is the Eulerian velocity at the boundary Γ, the Reynolds transport theorem generalizes the Leibniz's rule to multidimensional integrals as follows

$$\frac{\partial}{\partial t}\left(\int_{\Omega} f\,d\Omega\right) = \int_{\Omega}\frac{\partial f}{\partial t}d\Omega + \int_{\Gamma} f\,\mathbf{V}_{\Gamma}\bullet\mathbf{n}\;d\Gamma \tag{A2}$$

## 9. References


Banwait, SS. & Chandrawat, HN. (1998). Study of thermal boundary conditions for a plain journal bearing. *Tribol. Int.*, Vol. 31, No. 6, pp. 289–296, ISSN: 0301-679X

Bathe, K.-J. (1996). *Finite Element Procedures*, Prentice-Hall, ISBN: 0-13-301458-4 1, Upper Saddle River, New Jersey

Booker, J. F. & Huebner, K. H. (1972). Application of Finite Element Methods to Lubrication: An Engineering Approach. *ASME J. Lubr. Technol.*, Vol. 94, pp. 313–323 , ISSN: 0022-2305

Bonneau, D. & Hajjam, M. (2001). Modélisation de la rupture et de la formation des films lubrifiants dans les contacts élastohydrodynamiques. *Revue Européenne des Eléments Finis,* Vol. 10, No. 6-7, pp. 679-704, ISSN : 1250-6559

Bouyer, J. & Fillon, M. (2004). On the Significance of Thermal and Deformation Effects on a Plain Journal Bearing Subjected to Severe Operating Conditions. *ASME J. Tribol.*, Vol. 126, No. 4, pp. 819-822, ISSN: 0742-4787

Brugier, D. & Pasal, M.T. (1989). Influence of elastic deformations of turbo-generator tilting pad bearings on the static behavior and on the dynamic coefficients in different designs. *ASME J. Tribol.*, Vol. 111, No. 2 , pp. 364–371, ISSN: 0742-4787

Chang, Q.; Yang, P.; Meng, Y. & Wen, S. (2002). Thermoelastohydrodynamic analysis of the static performance of tilting-pad journal bearings with the Newton–Raphson method. *Tribol. Int.*, Vol. 35, No. 4, pp. 225-234, ISSN: 0301-679X

Dowson, D. (1967). A Generalized Reynolds Equation for Fluid-Film Lubrication. *Int. J. Mech. Sci.*, Pergamon Press Ltd., Vol. 4, pp. 159-170

Floberg, L. & Jakobsson, B. (1957). The finite journal bearing considering vaporization. *Transactions of Chalmers University of Technology*, Vol. 190, Gutenberg, Sweden

Fatu, A.; Hajjam, M. & Bonneau, D., (2006). A new model of thermoelastohydrodynamic lubrication in dynamically loaded journal bearings. *ASME J. Tribol.*, Vol. 128, pp. 85–95, ISSN: 0742-4787

Glavatskikh, S. (2001). Steady State Performance Characteristics of a Tilting Pad Thrust Bearing, *ASME J. Tribol.*, Vol. 123, No. 3, pp. 608-616, ISSN: 0742-4787

Kelly, D.W.; Nakazawa, S. & Zienkiewicz, O.C. (1980). A Note on Upwinding and Anisotropic Balancing Dissipation in Finite Element Approximations to Convective Diffusion Problems. *Int. J. Numer. Meth. Eng.*, Vol. 15, pp. 1705-1711, ISSN: 0029-5981

Kim, B.J. & Kim, K.W. (2001). Thermo-elastohydrodynamic analysis of connecting rod bearing in internal combustion engine, ASME J. Tribol., Vol. 123, pp. 444–454, ISSN: 0742-4787

Khonsari, M.M. & Booser, E.R. (2008). *Applied tribology: bearing design and lubrication*, Second Edition, Wiley & Sons, ISBN: 9780470057117, Chichester, UK

Kumar, A. & Booker, J.F. (1991). A finite element cavitation algorithm: Application/validation. *ASME J. Tribol.*, Vol. 107, pp. 253-260, ISSN: 0742-4787

Kumar, A. & Booker, J.F. (1994). A Mass and Energy Conserving Finite Element Lubrication Algorithm. *ASME J. Tribol.*, Vol. 116 , No. 4, pp. 667-671, ISSN: 0742-4787

LaBouff, G.A. & Booker, J.F. (1985). Dynamically Loaded Journal Bearings: A Finite Element Treatment for Rigid and Elastic Surfaces. *ASME J. Tribol.,* Vol. 107, pp. 505-515, ISSN: 0742-4787

Lund, J.W. & Tonnesen J. (1984). An approximate analysis of the temperature conditions in a journal bearing. Part II: Application. *ASME J. Tribol.*, Vol. 106, pp. 237–245, ISSN: 0742-4787

Kucinski, B.R.; Fillon, M.; Frêne, J. & Pascovici, M. D., (2000). A transient Thermoelastohydrodynamic study of steadily loaded plain journal bearings using finite element method analysis, *ASME J. Tribol.,* Vol. 122, pp. 219-226, ISSN: 0742-4787

Murty, K.G. (1974). Note on a Bard-type Scheme for Solving the Complementarity Problem. *Opsearch*, Vol. 11, pp. 123-130

Olsson, K. O. (1965). Cavitation in dynamically loaded bearing. *Transactions of Chalmers University of Technology*, Vol. 308, Guthenberg, Sweden

Piffeteau, S.; Souchet, D. & Bonneau, D. (2000). Influence of Thermal and Elastic Deformations on Connecting-Rod End Bearing Lubrication Under Dynamic Loading. *ASME J. Tribol.*, Vol. 122, No. 1, pp. 181-191, ISSN: 0742-4787

Robinson, C.L. & Cameron, A. (1975). Studies in hydrodynamic thrust bearings. *Philos. Trans.*, Vol. 278, No. 1283, pp. 351–395, ISSN: 1364-503X

Stefani, F. & Rebora, A. (2009). Steadily loaded journal bearings: Quasi-3D mass–energy-conserving analysis. *Tribol. Int.*, Vol. 42, No. 3, pp. 448-460, ISSN: 0301-679X

Stieber, W. (1933). Das Schwimmlager. *VDI*, Berlin

Swift, H. W. (1932). The stability of lubricating films in journal bearings. *Proc. Inst. Civil Eng.*, Vol. 233, pp. 267–288

Tezduyar, T. & Sunil, S. (2003). Stabilization Parameters in SUPG and PSPG formulations. *Journal of Computational and Applied Mechanics*, Vol. 4, No. 1, 7 pp. 1-88, ISSN: 15862070

Wang, Y.; Wang, Q.J. & Lin, C. (2003). Mixed Lubrication of Coupled Journal-Thrust-Bearing Systems Including Mass Conserving Cavitation. ASME *J. Tribol.*, Vol. 125, pp. 747-756, ISSN 0742-4787

Wendt, F. (1933). Turbulente stromungen zwischen zwei rotierenden konaxialen zylindern. *Ingenieur-Archiv,* Vol. 4, No. 3, pp. 577–595

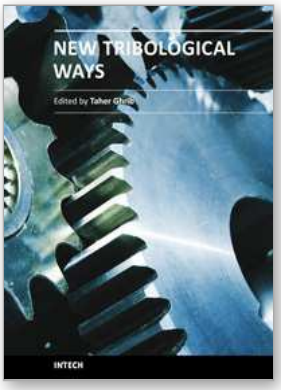


**New Tribological Ways**

Edited by Dr. Taher Ghrib

ISBN 978-953-307-206-7
Hard cover, 498 pages
**Publisher** InTech
**Published online** 26, April, 2011
**Published in print edition** April, 2011

This book aims to recapitulate old information's available and brings new information's that are with the fashion research on an atomic and nanometric scale in various fields by introducing several mathematical models to measure some parameters characterizing metals like the hydrodynamic elasticity coefficient, hardness, lubricant viscosity, viscosity coefficient, tensile strength .... It uses new measurement techniques very developed and nondestructive. Its principal distinctions of the other books, that it brings practical manners to model and to optimize the cutting process using various parameters and different techniques, namely, using water of high-velocity stream, tool with different form and radius, the cutting temperature effect, that can be measured with sufficient accuracy not only at a research lab and also with a theoretical forecast. This book aspire to minimize and eliminate the losses resulting from surfaces friction and wear which leads to a greater machining efficiency and to a better execution, fewer breakdowns and a significant saving. A great part is devoted to lubrication, of which the goal is to find the famous techniques using solid and liquid lubricant films applied for giving super low friction coefficients and improving the lubricant properties on surfaces.

**How to reference**

In order to correctly reference this scholarly work, feel free to copy and paste the following:

Fabrizio Stefani (2011). FEM Applied to Hydrodynamic Bearing Design, New Tribological Ways, Dr. Taher Ghrib (Ed.), ISBN: 978-953-307-206-7, InTech, Available from: http://www.intechopen.com/books/new-tribological-ways/fem-applied-to-hydrodynamic-bearing-design

INTECH
open science | open minds

**InTech Europe**
University Campus STeP Ri
Slavka Krautzeka 83/A
51000 Rijeka, Croatia
Phone: +385 (51) 770 447
Fax: +385 (51) 686 166
www.intechopen.com

**InTech China**
Unit 405, Office Block, Hotel Equatorial Shanghai
No.65, Yan An Road (West), Shanghai, 200040, China
中国上海市延安西路65号上海国际贵都大饭店办公楼405单元
Phone: +86-21-62489820
Fax: +86-21-62489821